

Evaluating and Improving Semi-analytic modeling of Dust in Galaxies based on Radiative Transfer Calculations II: Dust Emission in the Infrared.

Fabio Fontanot^{1,2} & Rachel S. Somerville^{3,4}

¹*INAF-Osservatorio Astronomico, Via Tiepolo 11, I-34131 Trieste, Italy*

²*MPIA Max-Planck-Institute für Astronomie, Königstuhl 17, 69117 Heidelberg, Germany*

³*Space Telescope Science Institute, 3700 San Martin Drive, Baltimore, MD 21218, USA*

⁴*Johns Hopkins University, Baltimore, MD 21218, USA*

email: fontanot@oats.inaf.it

Accepted ... Received ...

ABSTRACT

Interstellar dust grains are responsible for modifying the spectral energy distribution (SED) of galaxies, both absorbing starlight at UV and optical wavelengths and converting this energy into thermal emission in the infrared. The detailed description of these phenomena is of fundamental importance in order to compare the predictions of theoretical models of galaxy formation and evolution with the most recent observations in the infrared region. In this paper we compare the results of GRASIL, a code explicitly solving for the equation of radiative transfer in a dusty medium, with the predictions of a variety of IR template libraries, both analytically and observationally determined. We employ star formation history samples extracted from the semi-analytical galaxy formation model MORGANA to create libraries of synthetic SEDs from the near- to the far-infrared. We consider model predictions at different redshift ranges to explore any possible influence in the shape and normalization of the SEDs due to the expected evolution of the galaxy properties. We compute the total absorbed starlight predicted by GRASIL at optical wavelengths to statistically compare the synthetic SEDs with the selected IR templates. We show that synthetic SEDs at a given total infrared luminosity are predicted to be systematically different at different redshift and for different properties of the underlying model galaxy. However, we determine spectral regions where the agreement between the results of radiative transfer and IR templates is good in a statistical sense (i.e. in terms of the luminosity functions). Moreover, we highlight some potentially relevant discrepancies between the different approaches, both in the region dominated by PAH emission and at sub-mm wavelengths. These results determine potentially critical issues in the infrared luminosity functions as predicted by semi-analytical models coupled with different IR flux estimators.

Key words: galaxies: evolution - galaxies: dust

1 INTRODUCTION

The great advance in our understanding of the spectral energy distributions (SEDs) of galaxies has clearly demonstrated the ubiquitous presence of dust in galaxies. Dust plays a major role in galaxy evolution: it contributes to setting the physical conditions for star formation in galaxies, both seeding the formation of molecules and shielding the molecular gas from ionizing radiation. It is also important in the processes of cooling and condensation of giant molecular clouds (MCs) to the densities required for the onset of star

formation (see Dorschner & Henning 1995, for a review). At the same time, the presence of dust has a strong impact on the intrinsic spectral energy distributions (SED) of galaxies, since dust grains efficiently absorb and scatter radiation at short wavelengths ($\lambda < 1\mu m$). The absorbed energy is then thermally re-emitted at longer wavelengths in the infra-red (IR) region ($\lambda > 1\mu m$).

Dust-related processes of attenuation and re-emission are key mechanisms in understanding and interpreting galactic SEDs. Estimates based on the results of the IRAS satellite demonstrated that the IR region is responsible for

at least $\sim 30\%$ of the bolometric luminosity of nearby galaxies (Popescu & Tuffs 2002). Early IR surveys (see, e.g. Sanders & Mirabel 1996) discovered a population of heavily obscured luminous and ultra-luminous infrared galaxies (LIRGs, with IR luminosities $L_{IR} \sim 10^{11} - 10^{12} L_{\odot}$, and ULIRGs, $L_{IR} > 10^{12}$). Moreover, the study of the cosmic infrared background (see Hauser & Dwek 2001, for a review) shows that the global energy emitted in the IR is comparable to the direct starlight emission, detectable mainly at optical wavelengths, emerging from galaxies. Moreover, galaxy number counts in the mid-IR are an order of magnitude higher than those predicted by non-evolving local luminosity functions (Pozzetti et al. 1998; Elbaz et al. 1999; Lagache et al. 1999). Several groups (Chary & Elbaz 2001; Dole et al. 2001; Lagache et al. 2003) have shown that all these pieces of evidence favor strong evolution of the bright IR sources. This has been confirmed with direct observations of high-redshift sources using facilities like ISO (Dole et al. 2001; Elbaz et al. 2002; Gruppioni et al. 2002), the Spitzer Space Telescope (Le Floch et al. 2005; Babbidge et al. 2006) and SCUBA (Chapman et al. 2003, 2005). This strong evolution of luminous IR sources can also account for the peak in the cosmic infrared background.

Dust reprocessed radiation therefore represents a fundamental aspect of galactic emission: in particular a significant fraction of star formation activity is expected to be heavily extinguished and detectable only in the IR, since the molecular clouds are both the sites for star formation and among the most dusty environments. Most interestingly, this contribution was probably more important at higher redshift, where star formation activity and dust reprocessing are both stronger. The detailed modeling of dust properties is then a key issue in order to understand galaxy evolution at different cosmic epochs. Our understanding of these processes is complicated by the strong dependence of galactic SEDs on the relative geometry between dust and stars (Granato et al. 2000; Tuffs et al. 2004). In fact, the youngest stars, which dominate the UV luminosity, are expected to be heavily extinguished by their optically thick parent Molecular Clouds (MC). Older stars survive the disruption of the MCs and in fact, an age-dependent extinction has been postulated in the cirrus component for the intermediate-age stars (Popescu et al. 2000; Panuzzo et al. 2007), in order to reproduce the observed properties of disc-dominated galaxies. The emerging SED depends critically on the temperature distribution in the different environments (cirrus and MCs), as different dust species (with different composition and size) respond differently to the radiation field.

Therefore, a detailed treatment of the effects of dust grains in different spectral regions (both attenuation in the optical and re-emission in the IR) is of fundamental importance in order to infer the physical properties of galaxies from multi-wavelength observations and, conversely, to simulate galaxy UV-to-IR fluxes and colors from the predictions of theoretical models, both semi-analytic and numerical simulations. Semi-analytic models (SAMs, e.g., Bower et al. 2006; Croton et al. 2006; De Lucia et al. 2006; Monaco et al. 2007; Somerville et al. 2008) simulate the formation and evolution of galaxies, moving from a statistical description of the evolution of the Dark Matter structure (“merger trees” either analytically determined or extracted from the predictions of numerical simulations)

and using a well defined set of simple, but physically motivated, analytic “recipes” to describe the evolution and interplay of the various processes acting on the baryonic component (i.e. gas cooling and infall, star formation, stellar and AGN feedback). SAMs provide detailed information on the physical properties of model galaxies (in terms of star formation and AGN activity, stellar mass and gas mass content, stellar and gas metallicity) and some information on the relative geometry of the system (the sizes of the disc and bulge components). However, little, if any, information is available on the relation between dust mass and gas and metal content, as well as on the relative geometry between stars and dust and on the dust properties (grain size distribution and composition). Stellar population synthesis codes (e.g., Fioc & Rocca-Volmerange 1997; Silva et al. 1998; Leitherer et al. 1999; Bruzual & Charlot 2003) are then coupled with the star formation histories predicted by the SAM to produce synthetic spectra and photometry for the unattenuated starlight. The various codes presented in the literature show reasonable agreement on the intrinsic (pure-stellar) galactic SEDs, but they differ in the treatment of the highly complex effects of dust.

This paper is the second in a series aimed at better understanding and characterizing the different approaches for determining dusty SEDs in the SAM framework. In a Paper I (Fontanot et al. 2009, hereafter F09) we studied the effect of different prescriptions for dust attenuation at ultra-violet and optical wavelengths. In this paper we will instead focus on the re-emission of the absorbed energy in the infrared region (from $2\mu m$ to the sub-mm). Assuming that all energy absorbed by the dust at UV and optical wavelengths is re-radiated in the IR, it is possible to predict the expected IR fluxes in the region of interest. The approaches that have been used to date can be divided into two broad categories: those that use codes explicitly solving the equations of radiative transfer (RT) in a dusty medium, and those that make use of analytically motivated and/or empirically calibrated IR template libraries. Clearly the two approaches differ in the complexity and (therefore) in the computational effort involved in the treatment of dust effects. RT-solver methods of course provide more detailed predictions and a more correct dependence on the physical properties and geometrical configurations of dust in galaxies. However, the use of a full RT-solver coupled to a SAM substantially reduces the efficiency and flexibility of the semi-analytic approach (becoming the bottleneck of the computation, see e.g. Fontanot et al. 2007). Furthermore, this approach requires, and is sensitive to, a large number of additional parameters (specifying the details of the dust model) which must still be chosen somewhat empirically and which carry along numerous assumptions (such as constancy with redshift and/or environment). Given these drawbacks, and bearing in mind the large number of uncertainties and approximations already inherent in the SAM modeling, it is worth asking whether the difference between the results obtained with a full RT treatment versus IR templates justifies the use of the former tool.

IR templates are usually built up by combining the results of analytic calculations (Desert et al. 1990; Dale & Helou 2002; Lagache et al. 2004) and/or available observational constraints (Chary & Elbaz 2001; Rieke et al. 2009). They are then calibrated by means of comparison

with a well defined set of low- z objects. It is therefore unclear to which extent the same templates provide a good description of the SED properties at higher redshifts: several authors (see e.g. Rieke et al. 2009) discuss possible limitations in using these templates outside the redshift range on which they are calibrated. In the light of the previous discussion, we set out here to address a number of issues. First we briefly recap the study that we carried out in Paper I, in order to understand how well the amount of light absorbed by dust is predicted by analytic recipes for dust attenuation compared with a RT-solver. Our main goal is then to compare, on a statistical basis, the SED shapes contained in various IR template libraries from the literature with the predictions of a full RT solver coupled with a SAM and dust model. Both aspects of SED modeling will be of fundamental importance, given the growing interest triggered by infrared observations and the future availability of large datasets, thanks to facilities like the Herschel satellite. As a final goal for this project, we identify critical spectral regions, where the choice between RT-solver and IR templates may bias the comparison of model predictions with available observational data. To achieve these goals, we make use of the GRASIL RT code coupled with the MORGANA semi-analytic model. We derive a set of IR SED templates from the coupled MORGANA+GRASIL outputs, binned as a function of bolometric luminosity, and compare these with a range of templates from the literature. Finally, we compare the IR luminosity functions predicted by the full MORGANA+GRASIL runs with those that we obtain if we substitute the template approach.

This paper is organized as follows. In sec. 2.1 we describe the main features of the MORGANA and GRASIL models and we review the procedure used in F09 to define the synthetic RT-based SED libraries that we will use in the comparison. We introduce the IR template libraries in sec. 2.3 and we summarize the main results of F09 in sec. 2.4. In sec. 3.2 we present the statistical comparison between the properties of the RT-based SEDs and the IR templates, while in sec. 3.3 we discuss the effect of the different prescriptions on the statistical properties of model galaxies through the analysis of IR luminosity functions. Finally in section 4 we present our conclusions.

2 GALAXY MODELS

2.1 Semi-analytic model: MORGANA

We make use of the semi-analytic model MORGANA, developed by (Monaco et al. 2007) and Fontanot et al. (2007). We refer the reader to these papers and F09 for more details on the galaxy formation model, and here we just recall its main features: the model implements a sophisticated treatment of mass and energy flows between the different gas phases (cold, hot and stars) and galactic components (bulge, disc and halo), as well as a new treatment for gas cooling and infall (following Viola et al. 2008). It also includes both a multi-phase description of star formation and feedback (following Monaco 2004) and a self consistent description of AGN activity and feedback (Fontanot et al. 2006). For consistency with F09, we use the same star formation histories

(SFHs) and SED samples¹, extracted from the MORGANA (Monaco et al. 2007) realization presented in Fontanot et al. (2007). In this study we are mainly interested in the IR emission due to the coupling of stellar activity with the dusty interstellar medium, and we do not explicitly include the contribution of the central AGN to the predicted SEDs. This particular MORGANA realization assumes a Salpeter (1955) Initial Mass Function with mass range from 0.1 to 100 M_{\odot} .

Every model galaxy is represented assuming a composite geometry including both a spheroid and a disc component. Disc exponential profiles are computed following the Mo et al. (1998) formalism: the spin parameter of the DM halo is randomly extracted from a well defined distribution and the angular momentum is conserved. Bulge sizes are computed assuming that the kinetic energy is conserved in merger events (Cole et al. 2000). The presence of a bulge is taken into account when disc sizes are computed. MORGANA provides predictions for the star formation history, metal enrichment, and mass assembly of each component separately. This information is then interfaced with the RT-solver GRASIL (Silva et al. 1998) in order to predict the resulting SED from the UV to the Radio. The MORGANA realization we consider is able to reproduce the local and $z = 1$ stellar mass function, the cosmic star formation history, the evolution of the stellar mass density, the slope and normalization of the Tully-Fisher relation for spiral discs, the redshift distribution and luminosity function evolution for K -band selected samples, and, more interestingly, the number counts of 850 micron selected sources. Despite these successes, the agreement between model predictions and observations of the apparent “downsized” trend of galaxy formation is still under debate (see Fontanot et al. 2007, 2009 for a complete discussion about “downsizing” trends and SAMs). It is well established that this model overpredicts the number of faint, low-mass galaxies at $z < 2$ (Fontana et al. 2006; Fontanot et al. 2009) and the space density of bright galaxies at $z < 1$ (Monaco et al. 2006). Moreover, it does not reproduce the observed levels of star formation activity as a function of stellar and halo mass in the local universe (Kimm et al. 2009).

Many relevant properties of galaxies show redshift evolution, including star formation rates, sizes, metal and dust content. In order to test the effects of the predicted changes in these physical quantities, we follow the same approach as in F09, i.e. we draw two different samples of SFHs from the MORGANA predictions: a low- z ($0.0 < z < 0.2$) and a high- z sample ($2 < z < 3$). In F09, model galaxies in each sample are also split into disc-dominated and bulge-dominated subsamples² to test the effect of the composite geometry. We check that the shape of the IR SED does not show any strong dependence on the details of the geometrical configuration and our results are not affected by the splitting. Unless otherwise explicitly stated, in the following we will lift this subdivision.

¹ In F09 we refer to these ensembles as *ML libraries*. For the sake of simplicity and to avoid further confusion with the definition of the IR template libraries, in the following we will simply refer to the SFHs we extract from MORGANA as *samples* (i.e. low- z and high- z samples).

² according to their bulge-to-total ratio, with a threshold value of 0.6

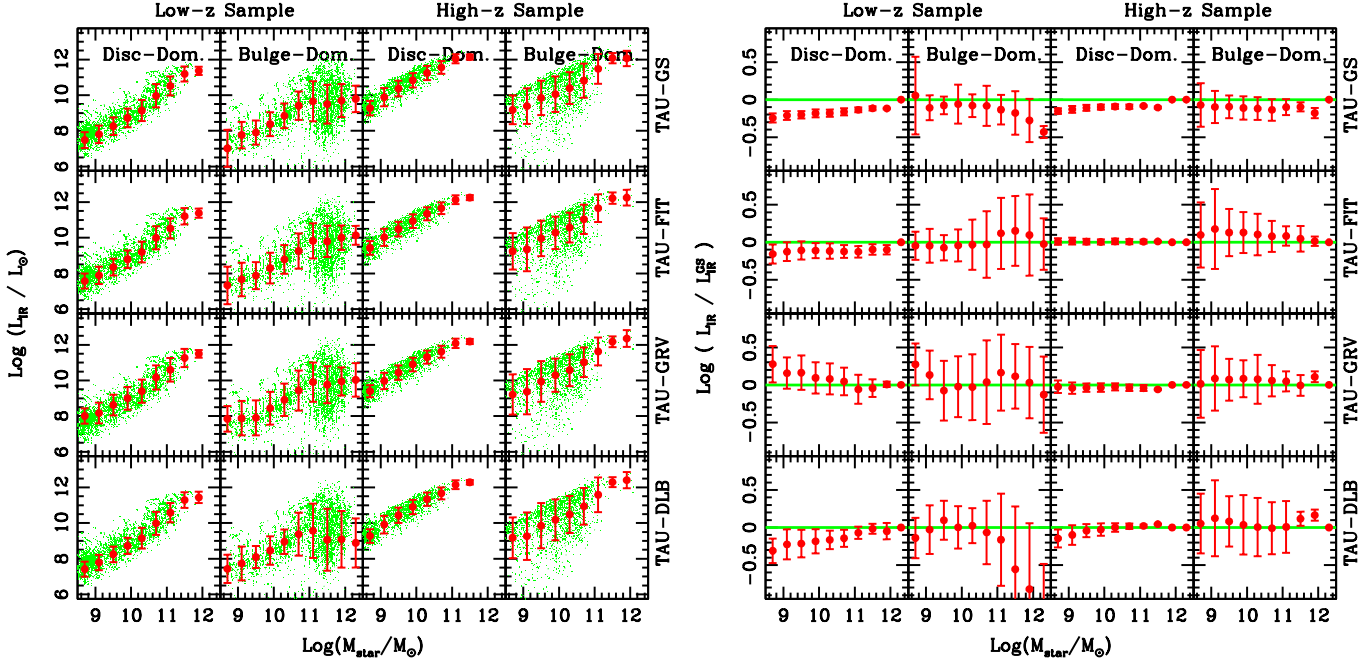


Figure 1. Left panels: absorbed starlight L_{IR} as a function of stellar mass for the objects in our samples. Green dots refer to the GRASIL results, while red circles with errorbars represent the mean predictions of the 4 prescriptions presented in F09, as indicated in the labels. Right panels: residuals in the relations (symbols and labels as in the left panels).

2.2 RT solver: GRASIL

For each object in our samples we interface MORGANA predictions with the spectro-photometric code GRASIL (Silva et al. 1998, for subsequent improvement we refer the reader to Silva 1999; Granato et al. 2000; Bressan et al. 2002; Panuzzo et al. 2003; Vega et al. 2005), to compute the corresponding SEDs from the UV to the Radio. GRASIL solves the equation of RT, taking into account a state-of-the-art treatment of dust effects. Stars and dust are distributed in a bulge (King profile) + disc (radial and vertical exponential profiles) axisymmetric geometry. The clumping of both (young) stars and dust through a two-phase interstellar medium with dense giant star-forming molecular clouds embedded in a diffuse (“cirrus”) phase are considered. The stars are assumed to be born within the optically thick MCs and to gradually escape from them on a time-scale t_{esc} , giving rise to age-(wavelength-) dependent extinction (i.e the youngest and most luminous stars suffer larger extinction than older ones). The dust composition consists of graphite and silicate grains (with a distribution of grain sizes), and Polycyclic Aromatic Hydrocarbons (PAH) molecules. At each point within the galaxy and for each grain type the appropriate temperature T is computed (either the equilibrium T for big grains or a probability distribution for small grains and PAHs³). The radiative transfer of starlight through dust is computed along the required line of sight yielding the emerging SED. The simple stellar population (SSP) library (Bressan et al. 1998, 2002) includes the effect of the dusty envelopes around AGB stars, and the radio emission from synchrotron radia-

tion and from ionized gas in HII regions. Although GRASIL computes the resulting SEDs along different lines of sight, in the following we use only angle-averaged SEDs.

Most of the physical information (such as stellar mass, star formation history, cold gas mass, gas metallicity) and parameters (scale radii for stars and dust in the disc and bulge components) needed by GRASIL are provided directly by MORGANA. We fixed the parameters used by GRASIL and not provided by MORGANA as in Fontanot et al. (2007) and F09. (i) The disc scale heights for stars and dust are set to 0.1 times the corresponding scale radii. (ii) We set the escape time-scale of young stars for the parent MCs to $t_{esc} = 10^7$ yr. This is a good compromise between the value needed to explain the SED of spirals (\sim a few Myr) and starbursts (Silva et al. 1998, \sim a few 10 Myr, see) and it is similar to the estimated destruction time scale of MCs by massive stars. In Fontanot et al. (2007) this value was found to produce good agreement with the K-band luminosity functions and the $850\mu\text{m}$ counts. (iii) The total gas mass is split between the dense and diffuse phases, assuming that 50% of the gas is in the star forming molecular clouds ($f_{MC} = 0.5$). The results are not very sensitive to this choice. (iv) The mass of dust is obtained by the gas mass and the dust-to-gas mass ratio δ_{dust} which is set to evolve linearly with the metallicity given by the galaxy model, $\delta_{dust} = 0.45 Z$. (v) The optical depth of MCs depends on the ratio $\tau_{MC} \propto \delta_{dust} M_{MC}/r_{MC}^2$; we set the mass and radius of MCs to typical values for the MW, $M_{MC} = 10^6 M_{\odot}$ and $r_{MC} = 16$ pc. (iv) The dust grain size distribution and composition is chosen to match the mean MW extinction curve.

Many authors have suggested that dust properties may evolve as a result of the evolution of galactic properties and/or differential metal enrichment (see e.g. Schurer et al.

³ The detailed PAH emission spectrum has been updated in Vega et al. (2005) based on the Li & Draine (2001) model.

2009). In a recent paper Lo Faro et al. (2009) analyzed the luminosity function of Lyman Break galaxies at $z > 3$ in the MORGANA framework, assuming the same GRASIL choices for the dust properties and their relation with gas and metal content. Their results show that the predicted extinctions are larger than the estimates of Bouwens et al. (2007). They then suggest that different values for t_{esc} and f_{MC} are able to reproduce the correct amounts of attenuation. Given the great uncertainties in the expected properties of dust as a function of redshift, we assume the same relations between dust and gas content, as well as the same dust composition and grain distribution for both the high- z and low- z sample. This assumption is similar in spirit to applying an IR template library derived from low-redshift observations at higher redshift. Thus, any differences that we find in the IR SEDs as a function of redshift are due to the changing physical properties of the model galaxies, not to changes in the dust properties. Given the strong dependence of the predicted SEDs on the details of the SFHs of model galaxies, the quantitative results we present in this paper are strictly valid only for the MORGANA+GRASIL algorithm, i.e. by interfacing GRASIL with another SAM, we expect to obtain a different sample of synthetic SED libraries. Nonetheless, the comparison between the predictions of these particular SED libraries and IR templates will provide us fundamental insight on the dependence of SAM predictions on the different IR modeling. Moreover, as shown in Fontanot et al. (2009), the global evolution of bulk galaxy properties (such as stellar masses and star formation rates) in GRASIL agrees well with other SAMs in the literature, suggesting that the results presented here would likely be similar for any currently available SAM.

2.3 IR template libraries

Starting from the pioneering work by Desert et al. (1990, hereafter DSP90), many authors proposed analytic solutions to RT equations, and used their results to define template IR SEDs as a function of L_{IR} , calibrated by comparison with known local prototypes. The original formulation of DSP90 assumed 3 main contributors to dust emission at IR wavelengths: polycyclic aromatic hydrocarbons (PAHs), very small grains and big grains. The former two are composed of graphite and silicates, with small and big grains probably dominated by graphite and silicate respectively. The thermal properties of each species are defined by its size distribution and its thermal state. Big grains are assumed to be in near thermal equilibrium. Their emission can be modeled as a modified black-body spectrum. On the contrary, small grains and PAHs are very likely in a state that is intermediate between thermal equilibrium and single photon heating. They are therefore subject to temperature fluctuations and their emission spectra are much broader than a modified black-body spectrum. The detailed size distributions are modeled using free parameters, which are calibrated by requiring the model to fit a series of observational constraints, such as the extinction/attenuation curves, observed IR colors and the IR spectra of local galaxies. Once the free parameters are fixed it is possible to use this model to predict the IR spectral contribution corresponding to each species, embedded in radiation fields of different intensity. The distribution of dust mass over heating intensity is usu-

ally assumed to follow a power-law (Dale et al. 2001, see, e.g.). The main advantage of this approach lies in the relatively small number of parameters required by the model (with respect to a RT solver). On the other hand, it relates a single SED to a class of model galaxies (defined by their infrared luminosity L_{IR}), irrespective of their morphologies or other properties.

In this paper we consider three different implementations of the DSP90 model, namely that proposed by Devriendt et al. (1999, hereafter DGS99), Dale & Helou (2002, hereafter DH02) and Lagache et al. (2004, hereafter L04). These implementations differ from the original DSP90 work, mainly in the modeling of the radiation field (DGS99, DH02), and in the relative contribution and shape of the IR emission of the different species (L04, DH02). The DGS99 template library consists of nine SEDs, corresponding to $L_{\text{IR}}^{\text{GS}}$ values spanning the range $10^6 L_{\odot} < L_{\text{IR}} < 10^{14} L_{\odot}$; L04 consists of five SEDs in the range $10^9 L_{\odot} < L_{\text{IR}} < 10^{13} L_{\odot}$; DH02 contains sixty-four SEDs in the range $2 \times 10^8 L_{\odot} < L_{\text{IR}} < 2 \times 10^{14} L_{\odot}$.

An alternative approach has been proposed by Chary & Elbaz (2001, hereafter CE01). They start from four reference SEDs generated using GRASIL and constrained to reproduce the observed SED of Arp220, NGC6090, M82 and M51 from the far-UV to the sub-mm (Silva et al. 1998). These four galaxies are considered representative of four galactic populations or luminosity classes: ULIRGs, LIRGs, starburst and normal galaxies respectively. They calibrate the $3\mu\text{m} < \lambda < 18\mu\text{m}$ region of the four model spectra with ISOCAM observations, then they split each SED into a mid-IR and a far-IR section and interpolate between the reference spectra to generate a set of sample template SEDs at intermediate luminosities. Additional templates from Dale et al. (2001) are used to widen the range of spectral shapes. The final templates are then chosen by requiring the two sections to account for a variety of observational constraints and merging together the best fit solutions in the two regions. The CE01 library consists of 105 templates, covering the range $2.7 \times 10^8 L_{\odot} < L_{\text{IR}} < 3.5 \times 10^{13} L_{\odot}$.

Finally, we also consider the recent work of Rieke et al. (2009, hereafter R09). They assemble detailed SEDs for eleven LIRGs and ULIRGs from observational datasets (including published ISO, IRAS and NICMOS data as well as previously unpublished IRAC, MIPS and IRS observations) and use them to build representative average IR templates. In regions where no homogeneous spectral coverage is available, they use GALAXEV (Bruzual & Charlot 2003) synthetic spectra, calibrated by requiring them to fit the available photometry. To model the far infrared SEDs, they assume a single black body with wavelength-dependent emissivity, while in the Radio they use a single power law wavelength dependence, as suggested by observed data. The R09 library includes fourteen SEDs covering the $5.6 \times 10^9 L_{\odot} < L_{\text{IR}} < 10^{13} L_{\odot}$ range.

2.4 Analytic Models of Dust Attenuation

In F09, we considered the effect of dust at optical to near-infrared wavelengths as predicted by GRASIL, by comparing the synthetic SED to the intrinsic starlight emission of each model galaxy. We compute mean dust attenuations and optical-to-near-infrared colors in the two samples

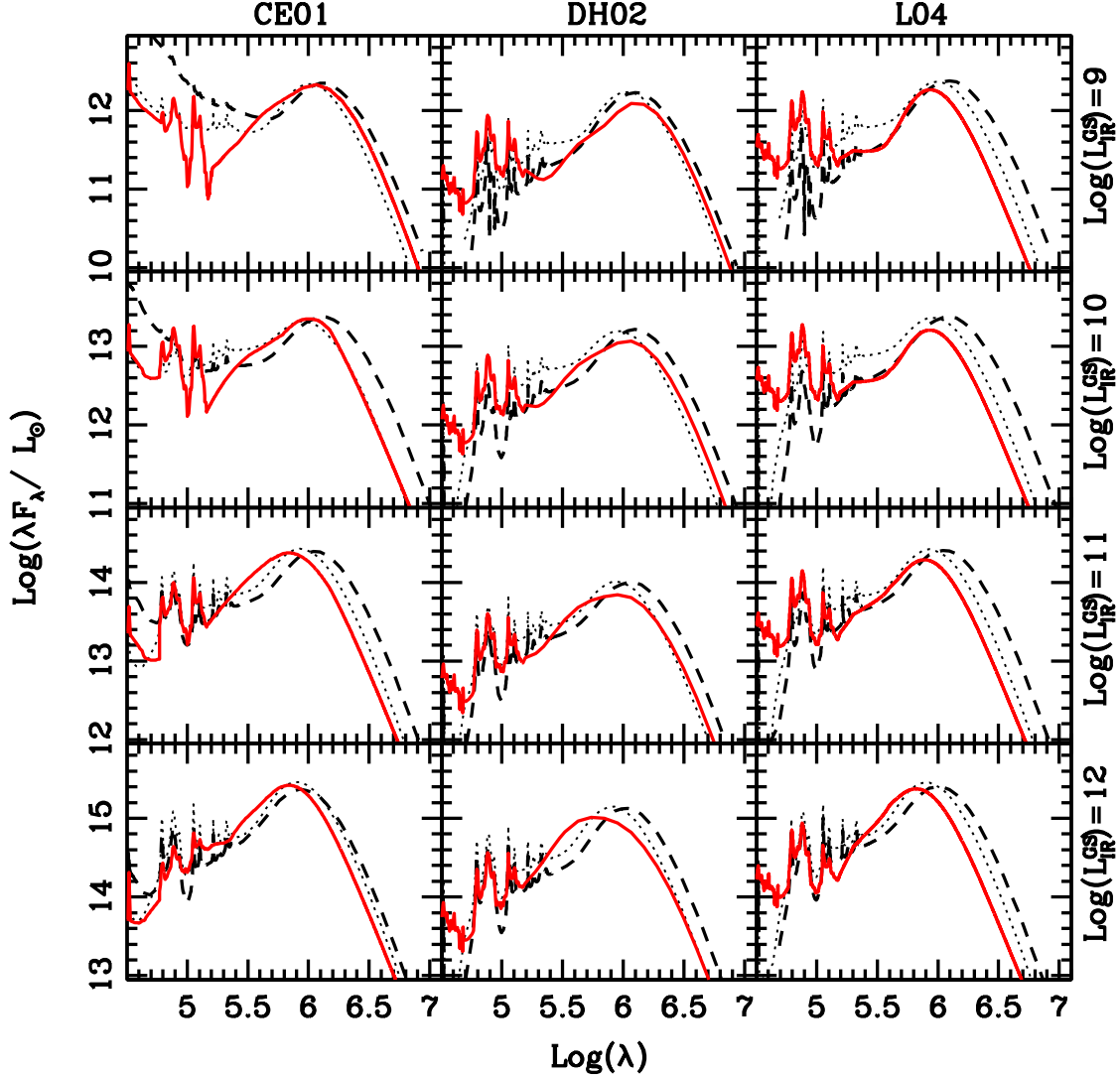


Figure 2. IR templates from the literature (red solid lines) compared to the GRASIL predicted mean SEDs for the CE01, DH02 and L04 libraries and four representative values of L_{IR} . In each panel the dashed and dotted lines refer to the low- z and high- z sample respectively. It is worth noting that the apparently different shapes of the mean SEDs in the various panels are due to the different L_{IR} binning considered in the original libraries (see text for more details).

and we then compare them to the predictions of simpler analytic prescriptions, commonly used in the SAM framework. These prescriptions are based on (i) an analytic attenuation law, normalized to (ii) an assumed value for the face-on optical depth at a reference wavelength (usually in the V-band, τ_V), eventually computed as a function of the physical properties of the galaxy itself; (iii) an inclination correction, performed by means of simple analytic models representing simplified geometries (such as the slab model or the oblate ellipsoid). In F09 we tested different choices and combinations of these three elements. In particular, we considered: (i) the Milky Way (Mathis et al. 1983), the Calzetti et al. (2000) and the age dependent Charlot & Fall

(2000) attenuation laws, plus the composite⁴ attenuation law of De Lucia & Blaizot (2007); (ii) the fitting formulae for τ_V proposed by Guiderdoni & Rocca-Volmerange (1987) and De Lucia & Blaizot (2007); (iii) slab and oblate ellipsoid geometries. Our results show that RT calculations can be reproduced with reasonable agreement even by a model as simple as a slab geometry combined with the composite age-dependent attenuation curve suggested by (De Lucia & Blaizot 2007), if an accurate estimate of the intrinsic τ_V is used to normalize the attenuation law. Using these synthetic SED samples, F09 tested different

⁴ i.e the Milky Way extinction curve describes the effect of the diffuse “cirrus” dust and the Charlot & Fall (2000) power-law the attenuation law experienced by young stars in the dense birth clouds.

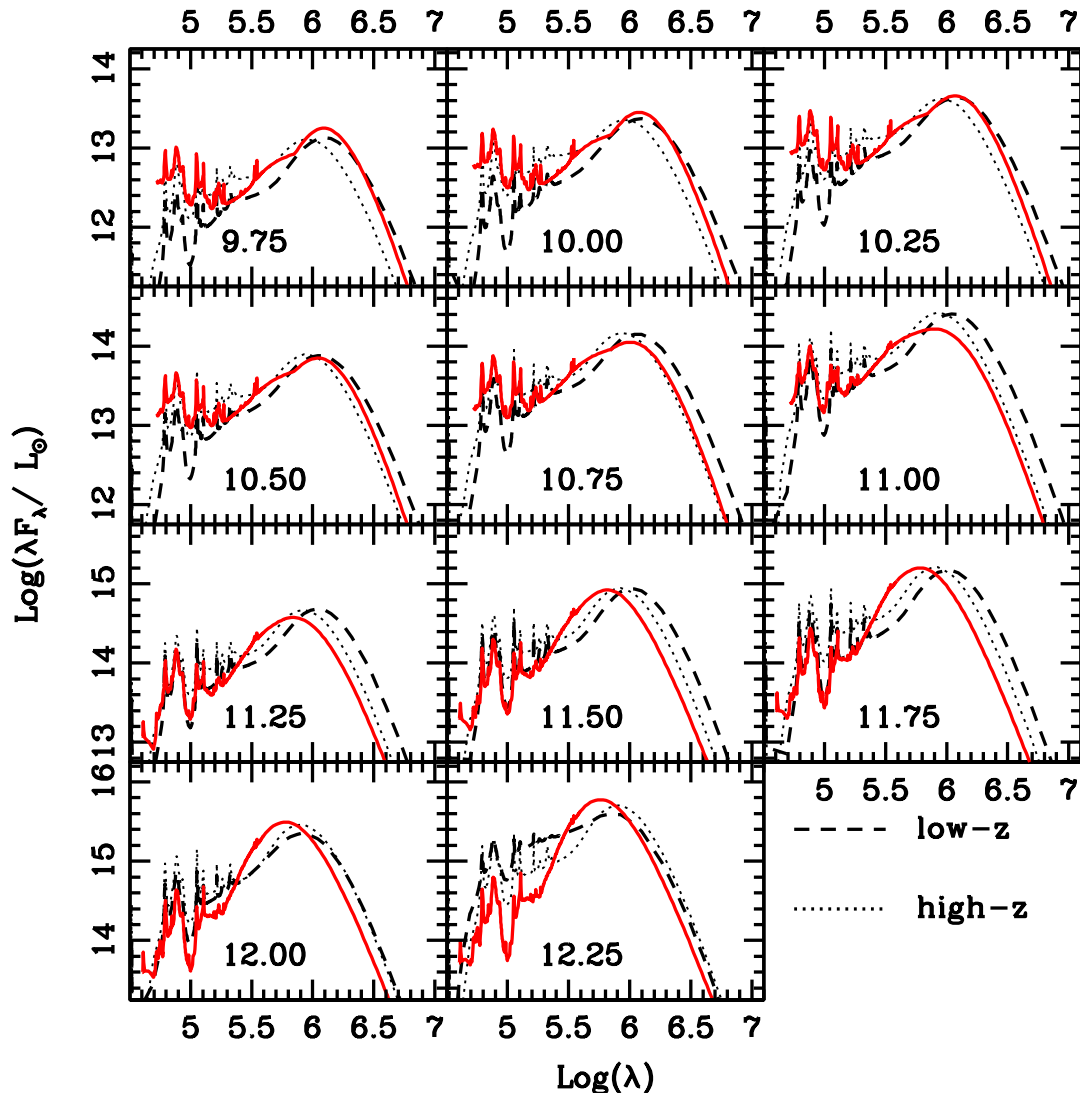


Figure 3. R09 IR templates (red solid lines) compared with the GRASIL predicted mean SEDs. In each panel the L_{IR} reference interval is indicated, while dashed and dotted lines refer to the low- z and high- z sample respectively.

analytic expressions, relating τ_V with the physical properties of the model galaxy (such as bolometric luminosity, stellar mass, metallicity, cold gas fraction and/or surface density). We demonstrated that the intrinsic value for τ_V , as predicted by GRASIL, correlates strongly with the gas metallicity, the cold gas mass and the scale radius of the model galaxies and we provided simple analytic fitting formulae. We then compared our formulae with analogous prescriptions found in the literature, and in particular with the the Guiderdoni & Rocca-Volmerange (1987) and De Lucia & Blaizot (2007) fitting formulae, by defining four different analytic prescriptions for dust attenuation and testing them against GRASIL predictions. The four prescriptions share the same choice for attenuation law and geometry (i.e. a De Lucia & Blaizot (2007) composite attenuation law combined with a slab model), but assume a different normalization (i.e. τ_V). A first prescription uses the intrinsic τ_V value as computed

from the comparison of attenuated and unextinguished GRASIL synthetic SEDs (TAU-GS). In the remaining we assume both the Guiderdoni & Rocca-Volmerange (1987) and De Lucia & Blaizot (2007) τ_V fitting formulae plus our results: we then define TAU-GRV, TAU-DLB and TAU-FIT prescriptions respectively. We showed that the agreement among the different prescriptions is satisfactory for the low- z sample, but the discrepancies are significant in the high- z sample. Our proposed fitting formulae provide the best compromise in reproducing the RT-predictions in both samples at the same time.

3 RESULTS

3.1 Total Absorbed Starlight

In this paper we extend the analysis of F09 by considering the energy re-emitted by dust at longer wavelength. There-

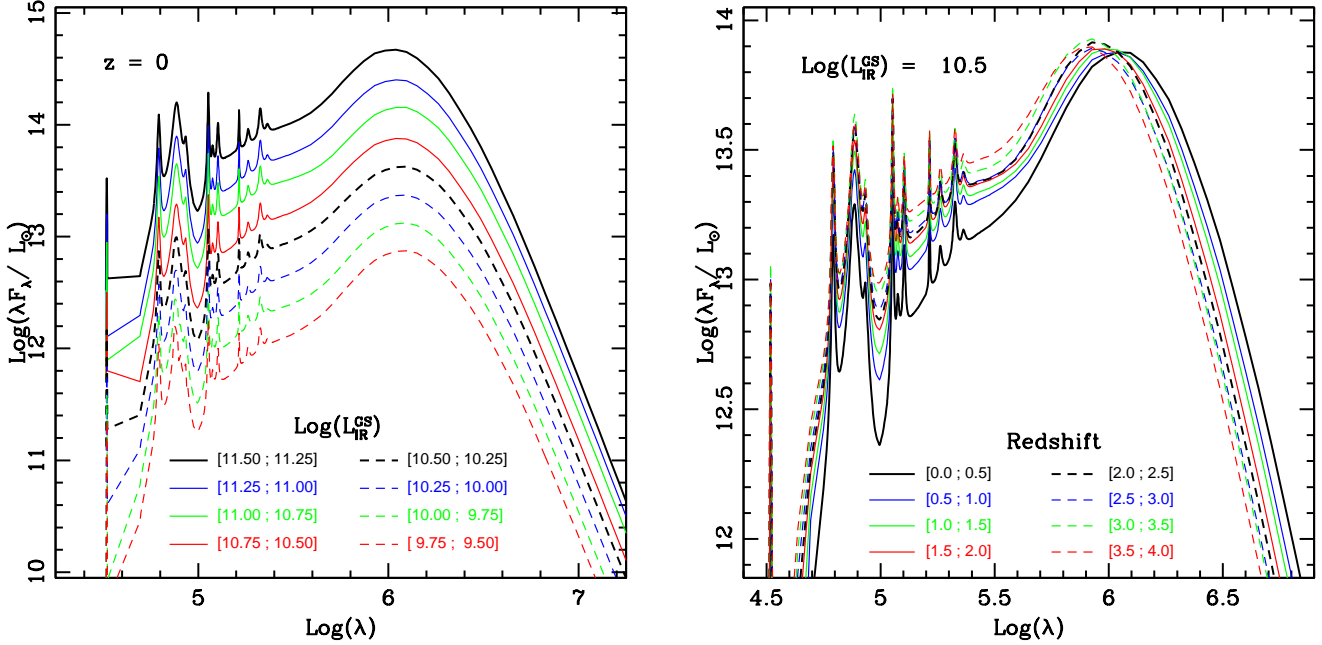


Figure 4. *Left Panel:* Mean SED evolution as a function of L_{IR} in the low- z sample. *Right Panel:* The evolution of GRASIL predicted mean SEDs as a function of redshift.

fore, as a first critical test we compare the total amount of absorbed starlight from the UV to the near-infrared (L_{IR}) both in GRASIL and in the four analytic extinction prescriptions. We compute the intrinsic value of L_{IR}^{GS} by comparing the extinguished F_{λ}^{abs} and unextinguished F_{λ}^{unabs} SEDs:

$$L_{IR}^{GS} = \int_{100nm}^{2200nm} (F_{\lambda}^{unabs} - F_{\lambda}^{abs}) d\lambda \quad (1)$$

Starting from F_{λ}^{unabs} and applying the four prescriptions for dust attenuation, we estimate the corresponding L_{IR} values. We compare them with L_{IR}^{GS} in fig. 1: in each case we see reasonable agreement between the predicted total amounts of absorbed starlight and GRASIL results. This encouraging result is not obvious, since our prescriptions assumed a fixed shape for the extinction law (even if we consider an age-dependent component). This implies a fixed ratio between the attenuation at different wavelengths. On the other hand, we showed in F09 (fig. 3) that the scatter in GRASIL predicted attenuation laws is significant, and although the Milky Way attenuation law is a good estimate for the mean shape, single objects may deviate considerably. The agreement is especially good for the disc-dominated objects, where we see a tight relation between the stellar mass and L_{IR}^{GS} . The intrinsic scatter increases in the bulge-dominated objects and the analytic prescription are able to reproduce the general trend, even if the residuals of the relation (right panels) show a 0.5dex scatter. This result suggests that the deviation of synthetic SEDs from a Milky Way attenuation law is larger in bulge-dominated objects. Under the hypothesis that all the absorbed energy is re-emitted at infrared wavelengths, and assuming a set of IR templates as described above, it is then possible to estimate the corresponding infrared SEDs.

3.2 Comparing IR SEDs

In order to compare the predictions of the full RT calculation to the IR template approach we split the model galaxies in the low- z and high- z samples into IR luminosity classes, according to their L_{IR}^{GS} . For each IR template library, we define luminosity classes by sorting each model galaxy into the nearest L_{IR} bin. We renormalize each GRASIL SED in our sample to the ratio between L_{IR}^{GS} and the L_{IR} of the bin. We then compute the statistical properties of the synthetic SEDs for each class: we create a mean SED, by considering the mean flux at each wavelength, and we define a scatter in the flux distribution as a function of wavelength. For the CE01 templates we consider both the contribution of direct starlight and dust emission, whereas for the other libraries we consider only the contribution of the dust emission. We consider the low- z and high- z samples separately.

We compare the mean GRASIL SEDs to the corresponding IR templates, for four representative values of L_{IR} and three libraries in fig. 2. The agreement between the mean SEDs constructed from our samples and the IR templates is satisfactory in most cases, but there are some significant discrepancies. In order to perform the same comparison over a wider range of L_{IR} , we consider the full dynamical range probed by the R09 library in fig. 3. The most prominent difference between the templates and the predictions of the RT-solver concerns the position of the peak of the thermal dust emission: the peak is shifted to longer wavelengths in the GRASIL predictions relative to the IR templates. It is particularly evident in fig. 3 that the discrepancy depends also on L_{IR} . In order to get a better insight into this problem, we compare the mean GRASIL SEDs for different values of the total amount of energy emitted in the IR in fig. 4 (left panel). L_{IR} has a strong effect on the overall normalization of the mean SEDs, but they show a quite similar shape. In

particular the position of the IR peak does not depend on L_{IR} over the whole range studied, while it is evident from fig. 3, that it is changing slightly in the templates. Since the position depends mainly on the temperature distribution of the emitting grains, this is likely connected to the modeling of dust abundance and distribution. We stress that we assume the same dust properties for all galaxies in the MORGANA+GRASIL realization (by fixing the related parameters to mean values, see sec. 2.2), a common assumption in the semi-analytic approach. Another notable discrepancy is present in the Mid-Infrared ($8\mu\text{m} < \lambda < 20\mu\text{m}$), where the highly uncertain contribution of PAH emission is dominant. Finally, it is also worth noting the strong discrepancy seen in most cases at the shortest wavelengths ($\lambda < 8\mu\text{m}$). This is the region where direct starlight emission from old stars is still significant in the galactic SEDs and comparable to the dust thermal emission: therefore we interpret this result as due to the difficulties in disentangling the relative contribution of these two components.

Another interesting insight from the analysis of fig. 2 and 3 is the different shapes of the mean SEDs drawn from the high- z and low- z sample. In most cases the mean SEDs corresponding to the high- z sample show on average a better agreement with the corresponding template. This result is somewhat surprising, given the fact that IR templates are calibrated using low- z observations. In order to better understand this result, we construct the mean SEDs over a finer binning in redshift, while retaining the same L_{IR} binning as for the R09 templates. We compare the evolution of the new mean SED sample with redshift in fig. 4 (right panel), for the representative luminosity bin centered at $\text{Log}(L_{IR}) = 10.5$. It is evident from this plot that the mean SED is experiencing a strong redshift evolution, in particular in the spectral regions corresponding to the peak of thermal IR emission and PAH emission. This pattern can be ascribed to the redshift evolution of the physical properties (i.e. gas content, metal enrichment and size evolution) of the model galaxies in the MORGANA realization and represents a warning against using the same template library over a wide redshift range (as already noticed by DN02 and R09). In order to get better insight into the main driver of the evolution of the SED shape, we perform a fitting procedure similar to F09 (see their sec. 4). For each synthetic SED in our library, we modeled the wavelength corresponding to the peak of IR emission as a power-law function of the physical properties of the corresponding model galaxy. We consider L_{IR} , the stellar and cold gas masses, the star formation rate, metallicity and galactic radius and we define a set of general relations involving independent quantities. For each combination, we determine the best-fit parameters and evaluate the goodness of the fit through a χ^2 procedure. Our results show that the strongest correlation is found for the total mass surface density of the galaxy. This is not completely unexpected since the relative spatial distribution of stars and gas is fundamental to predicting the temperature of dust grains. The scatter in the correlation is large, but we find that adding additional degrees of freedom does not reduce it considerably. We conclude that other physical quantities, like star formation rate and metallicity, still play a non-negligible role in determining the resulting shape of the SED.

We then consider the distribution of fluxes as a function

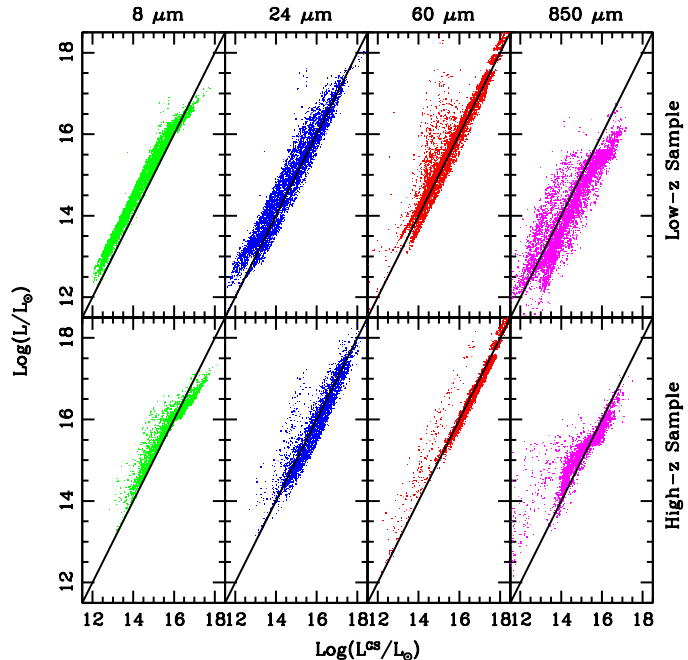


Figure 6. Intrinsic IR luminosities at 8, 24, 60, 850 μm compared with the corresponding predictions for the R09 templates.

of wavelength in fig. 5. It is evident from the plot that the scatter within each L_{IR} class may be important, especially at the lowest values of total absorbed starlight. Both the scatter variations between different libraries at a given L_{IR} (left panels) and along the same library (right panels) are mainly due to the inhomogeneous distribution of galaxies in the L_{IR} bins. As expected, larger binnings correspond to larger scatters around the mean SEDs. At the same time, the variance of the flux as a function of wavelength does not show any significant dependence on redshift, for a given L_{IR} bin. This result implies that using a single SED from a template library to describe all galaxies belonging to a given L_{IR} class, may introduce a bias between the comparison between model predictions and observations. Our analysis shows that it is possible to use mean SEDs as representative for all SEDs belonging to a luminosity class only in a statistical sense (and this proxy improves with finer binning in L_{IR}), but not on a object-by-object basis. It is also worth noting that the different binning has a non-negligible effect on the shape and normalization of the corresponding mean SED, due to the different sample definition. Although the IR templates share a similar trend, this is another hint that a finer binning helps reduce the differences between templates and RT predictions.

3.3 Effect on the IR Luminosity functions

We then compare the individual monochromatic luminosities for each model galaxy as predicted by the GRASIL computation and by the IR templates. We select four wavelengths widely used in the literature to track different galaxy populations and constrain the properties of dust and PAHs at different temperatures: namely the $8\mu\text{m}$, the $24\mu\text{m}$, the $60\mu\text{m}$ and the $850\mu\text{m}$ restframe luminosities. For each model

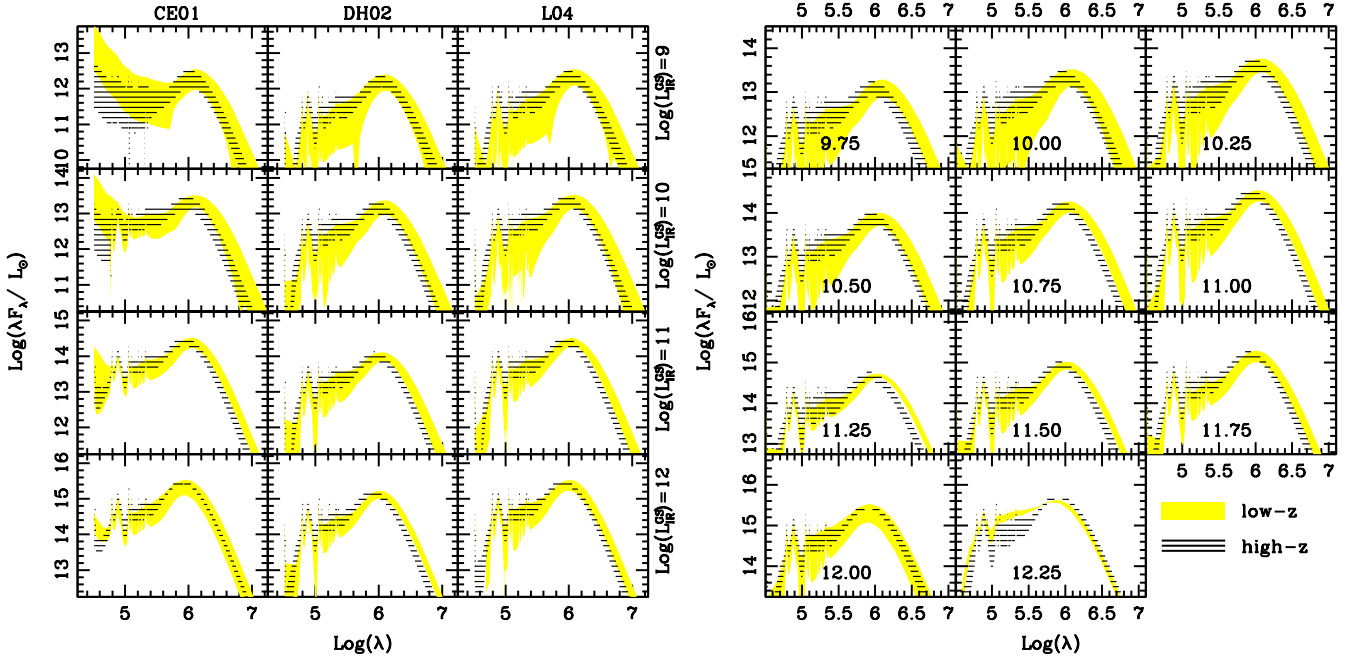


Figure 5. *Left Panels:* The 1- σ distribution of GRASIL predicted SEDs in the same L_{IR} reference intervals and for the same libraries as in fig 2. *Right Panels:* The 1- σ distribution of GRASIL predicted SEDs for the same L_{IR} reference intervals as defined in R09. The central L_{IR} value for each interval is indicated in each panel. In all panels the yellow shaded area and horizontal texture refer to the low- z and high- z sample respectively.

galaxy we estimate the expected fluxes from the IR template library as follows. We use the intrinsic GRASIL-predicted L_{IR}^{GS} to select the closest template for each IR library. We then rescale the template to the ratio between its L_{IR} and L_{IR}^{GS} , and we use it to estimate the monochromatic luminosities in the four bands. For the CE01 templates we simply use the template, while for the other libraries we sum up the chosen template with the extinguished starlight spectrum (as predicted by GRASIL). We then statistically compare the predictions derived using the template libraries with the intrinsic results of GRASIL computations by constructing the corresponding luminosity functions. In this way we are able to quantify the impact of the different choice for IR templates on the statistical properties of galaxy samples, as predicted by SAMs. It is worth stressing here that we do not require our SAM to reproduce the properties of the local Universe. Instead our aim is to check the impact of different prescriptions for dust emission on the predictions of SAMs.

In fig. 6 we show a comparison between the monochromatic luminosities obtained using the R09 templates with the intrinsic GRASIL predictions (similar results hold for the other templates), while in fig. 7 the resulting luminosity function for all considered templates (right panel). The intrinsic luminosity functions for our low- z and high- z samples are represented by the solid thick line, while other lines correspond to the predictions obtained using the four IR template libraries. We find similar results with respect to the analogous analysis at optical and near-infrared wavelengths presented in F09 (their fig. 12): both the shape and normalization of the luminosity functions are correctly recovered in most cases. However, in the sub-mm region, GRASIL fluxes are systematically underpredicted by the templates:

this is mainly due to the discrepancy in the position of the $\sim 100\mu\text{m}$ peak in the SEDs (see fig. 2), which affects the shape of the SEDs at longer wavelengths. In the low- z sample, the flux at $850\mu\text{m}$ is underpredicted only for the brightest sources, while at fainter fluxes the agreement is reasonable. However, in the high- z sample the templates are not able to reproduce the brightest sources at $8\mu\text{m}$, while the agreement at $24\mu\text{m}$ and $60\mu\text{m}$ is again satisfactory. It is possible to understand this peculiar behavior by looking at the shape of the brightest mean SEDs compared with the corresponding templates in fig. 2.

4 SUMMARY

This paper is the second in a series aimed at (i) understanding and quantifying the results of detailed calculations of radiative transfer in a dusty medium and (ii) comparing these results with simpler analytic recipes coupled with semi-analytic models and spectro-photometric codes. The final goal of this work is to assess the impact of different modeling for dust attenuation and emission in the framework of semi-analytic models of galaxy formation and evolution. In the first paper of the series (F09) we studied the effects of dust attenuation at optical and UV wavelengths, while in this paper we focus on the dust emission in the IR region. We use the same star formation history libraries based on the MORGANA semi-analytic model and defined in F09: they include a low- z ($0 < z < 0.2$) and a high- z ($2 < z < 3$) sample, with the aim of assessing the effect of the evolution of galaxy physical properties on the corresponding SEDs. We couple the star formation histories and galaxy properties to

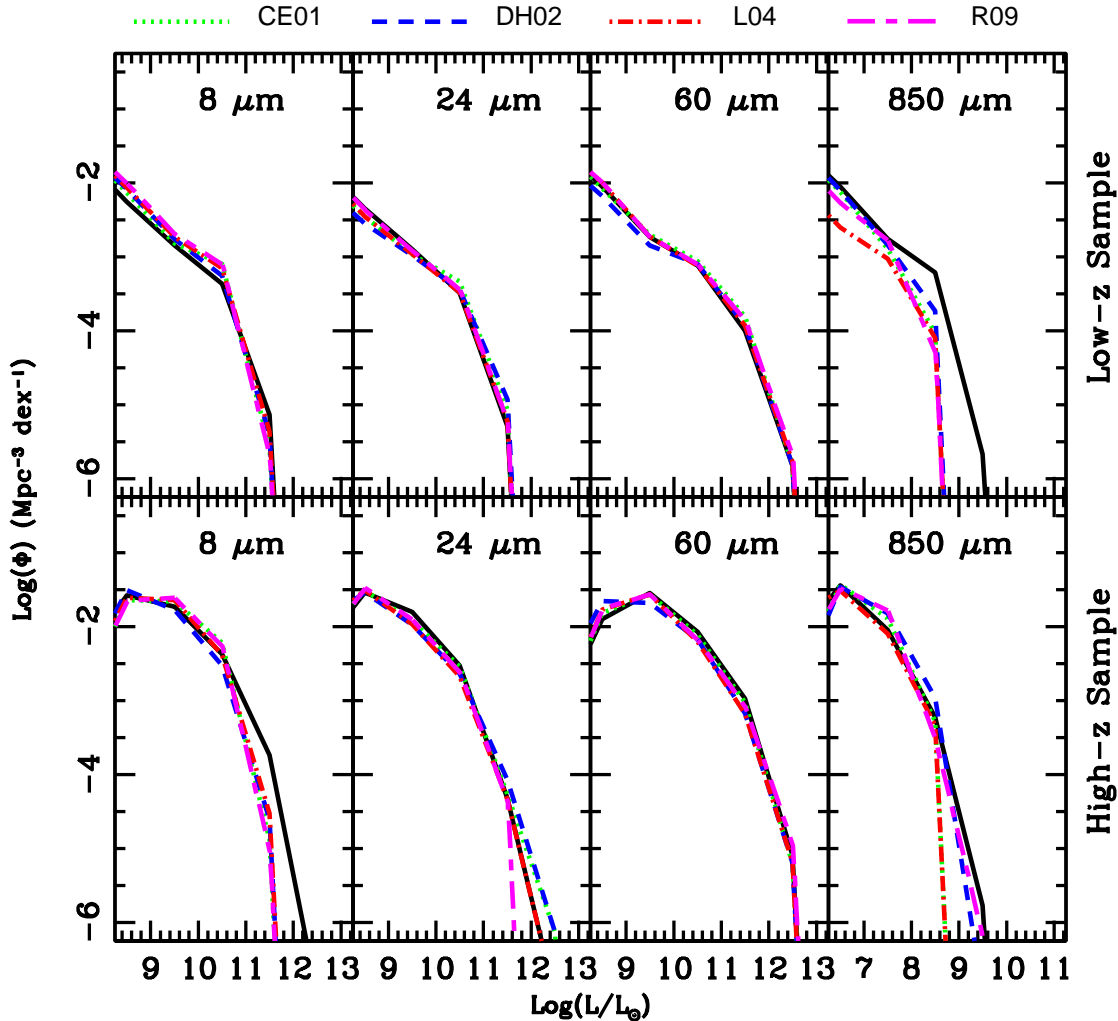


Figure 7. GRASIL predicted IR luminosity functions in the low- z and high- z samples (thick solid lines) compared with the predictions using the IR template libraries. Solid, dotted, dashed, dot-dashed and long-short dashed lines refer to GRASIL, CE01, DH02, L04 and R09 templates respectively.

the RT-solver GRASIL, to obtain an estimate of the synthetic SEDs from the UV to the Radio.

As a first check we consider the intrinsic absorbed starlight L_{IR} according to the GRASIL results and we compare it to the predictions of the four prescriptions for dust attenuation at optical to near-infrared wavelengths discussed in F09. As already shown in F09, the scatter in the GRASIL predicted attenuation laws is not negligible: therefore we expect discrepancies on an object-by-object basis. However, our results show that all prescriptions provide a reasonable description of the mean intrinsic L_{IR} for the whole population, within the errors shown in fig. 1. We conclude that such simplified analytic approaches can be used to obtain statistically valid estimates for L_{IR} .

We then consider four different IR template libraries, commonly coupled to spectro-photometric models to provide predictions for dust emission in the IR. They include both theoretical (Dale & Helou 2002; Lagache et al. 2004)

and empirical templates (Chary & Elbaz 2001; Rieke et al. 2009). In each case, we define L_{IR} classes similar to those used to generate the IR templates and we sort the synthetic SEDs for the low- z and high- z samples accordingly. For each class, we then construct mean SEDs by computing the mean fluxes as a function of wavelength. Our results show that, overall, the mean SEDs are in fairly good agreement with IR templates over a wide spectral range. Significant discrepancies arise both at wavelengths longer than the $\sim 100\mu\text{m}$ peak (due to the different positioning of the peak itself) and for low IR luminosities. Moreover, by comparing a low- z and a high- z sample we see significant differences in the properties of mean SEDs, again growing larger for low values of L_{IR} .

In order to gain better insight into the origin of these discrepancies, we compute mean SEDs on a finer binning in the L_{IR} and redshift space. We then consider the redshift evolution of the mean SED at a fixed L_{IR} (and vice

versa). The mean SED shape shows strong redshift evolution at fixed L_{IR} , and very little evolution as a function of L_{IR} at a given cosmic epoch. We quantify the dependence of the SED shape on the physical properties of the underlying model galaxies by fitting the position of the peak of IR emission. Our results show that the main contributor is the redshift evolution of the spatial distribution of stars and gas (total mass surface density) as predicted by MORGANA. Both star formation rate and metallicity cause a secondary, but non-negligible contribution to the broad scatter in the relation. This result reflects the fact that the main factor responsible for the detailed shape of the GRASIL predicted IR SED is the mean temperature of dust grains, which is a complex function of the distribution of dust particles (linked to the cold gas surface density and metallicity) and of the radiation field (linked to the stellar mass surface density and star formation rate).

These results suggest that it may not be valid to use the same IR template library for modeling galaxies at different redshifts, where the physical properties are likely different (as in the case of MORGANA galaxies). Moreover, despite the fact that many physical properties of galaxies (such as gas and metal content, present and past star formation activity, disc and bulge sizes) are predicted by the SAM, when solving the equation of RT we still have to make assumptions about the physical state of the dust (composition, grain size distribution) and about its distribution relative to stars and the inter-stellar medium. Given the present uncertainties, we assume that these properties do not change as a function of galactic properties nor with cosmic time over the redshift range we consider. Our choice reflects a parameter combination that has been proven adequate for reproducing the properties of $z < 3$ galaxies (Silva et al. 1998; Fontanot et al. 2007), and it explains the stability of mean SED shapes over a narrow redshift range. This implies that any variation in SED shape with redshift seen in our results reflects only the effects of galaxy evolution. However, a strong systematic variation of these parameters (especially t_{esc} and f_{MC}) at higher redshifts is expected both observationally (Maiolino et al. 2004) and theoretically (Lo Faro et al. 2009). We expect any variation in the dust parameters and/or composition (Schurer et al. 2009) to lead to even larger differences in the mean SED shape and normalization. Finally, we also show that the scatter around the mean fluxes is significant and it depends on the width of the L_{IR} binning. For a sparse sampling of L_{IR} the mean SEDs give only a poor description of the SED variety.

We then consider the IR monochromatic luminosities at $8\mu m$, $24\mu m$, $60\mu m$ and $850\mu m$ as predicted by the MORGANA+GRASIL model and by the four IR template libraries. We compare the fluxes on an object-by-object basis and the resulting luminosity functions. Although there are large discrepancies for some individual objects (up to two orders of magnitude), the overall statistical agreement is quite good in most regimes. There is a systematic discrepancy at $850\mu m$ for both the low- z and high- z samples, with a systematic underprediction of the RT predicted luminosity functions. This is mainly related to the discrepant position of the $\sim 100\mu m$ peak in the SEDs with respect to the templates. The brightest sources in the high- z sample show disagreement also at $8\mu m$, while the $24\mu m$ and $60\mu m$ predictions are similar. This is related to the peculiar shape of the high- z sample mean

SED at this IR luminosity, and, again, implies that caution should be used when comparing theoretical IR predictions from different methods, even on a statistical basis.

Our results extend those presented in F09 into the IR regime, and our conclusions are quite similar. The level of agreement between the predictions of a RT solver approach (superior in order to understand the details of dust absorption and re-emission in galaxies on a object-by-object basis) and more computationally efficient semi-analytic methods depends on the spectral regions under analysis. We have identified wavebands where the agreement is good (in a statistical sense) and others where the discrepancies are significant. In particular, for the MORGANA+GRASIL model the agreement between the two approaches is good in the Mid-IR, while we found significant discrepancies at $8\mu m$ and $850\mu m$.

As a wealth of multi-wavelength observations are becoming available in the IR, we expect to use them to constrain with greater accuracy the redshift evolution of dust properties and their relation with the physical properties of galaxies, as well as the observed shape of their SEDs over a wide range of redshift. It has been recently shown that the computational times required for a full RT solver coupled to a SAM can be considerably shortened, with no loss of accuracy, with the use of neural networks (Silva et al. 2010), thus relaxing one of the strongest problems connected to the use of this tool in the SAM framework. At the same time, improvements in the SAMs are needed, i.e. the modeling of dust generation, evolution and dispersion, in order to reduce the number of externally fixed parameters and make use of the full predictive power of RT solvers.

ACKNOWLEDGMENTS

The authors would like to thank Pierluigi Monaco and Gabriella de Lucia for stimulating discussions. Some of the calculations were carried out on the PIA cluster of the Max-Planck-Institut für Astronomie at the Rechenzentrum Garching. FF acknowledges the support of an INAF-OATs fellowship granted on 'Basic Research' funds and hospitality at the Kavli Institute for Theoretical Physics in Santa Barbara. This research was supported in part by the National Science Foundation under Grant No. NSF PHY05-51164.

REFERENCES

- Babbedge T. S. R., Rowan-Robinson M., Vaccari M., Surace J. A., Lonsdale C. J., Clements D. L., Fang F., Farrah D. e. a., 2006, MNRAS, 370, 1159
- Bouwens R. J., Illingworth G. D., Franx M., Ford H., 2007, ApJ, 670, 928
- Bower R. G., Benson A. J., Malbon R., Helly J. C., Frenk C. S., Baugh C. M., Cole S., Lacey C. G., 2006, MNRAS, 370, 645
- Bressan A., Granato G. L., Silva L., 1998, A&A, 332, 135
- Bressan A., Silva L., Granato G. L., 2002, A&A, 392, 377
- Bruzual G., Charlot S., 2003, MNRAS, 344, 1000
- Calzetti D., Armus L., Bohlin R. C., Kinney A. L., Koornneef J., Storchi-Bergmann T., 2000, ApJ, 533, 682

- Chapman S. C., Blain A. W., Ivison R. J., Smail I. R., 2003, *Nature*, 422, 695
- Chapman S. C., Blain A. W., Smail I., Ivison R. J., 2005, *ApJ*, 622, 772
- Charlot S., Fall S. M., 2000, *ApJ*, 539, 718
- Chary R., Elbaz D., 2001, *ApJ*, 556, 562
- Cole S., Lacey C. G., Baugh C. M., Frenk C. S., 2000, *MNRAS*, 319, 168
- Croton D. J., Springel V., White S. D. M., De Lucia G., Frenk C. S., Gao L., Jenkins A., Kauffmann G., Navarro J. F., Yoshida N., 2006, *MNRAS*, 365, 11
- Dale D. A., Helou G., 2002, *ApJ*, 576, 159
- Dale D. A., Helou G., Contursi A., Silberman N. A., Khatkar S., 2001, *ApJ*, 549, 215
- De Lucia G., Blaizot J., 2007, *MNRAS*, 375, 2
- De Lucia G., Springel V., White S. D. M., Croton D., Kauffmann G., 2006, *MNRAS*, 366, 499
- Desert F.-X., Boulanger F., Puget J. L., 1990, *A&A*, 237, 215
- Devriendt J. E. G., Guiderdoni B., Sadat R., 1999, *A&A*, 350, 381
- Dole H., Gispert R., Lagache G., Puget J.-L., Bouchet F. R., Cesarsky C., Ciliegi P., Clements D. L. e. a., 2001, *A&A*, 372, 364
- Dorschner J., Henning T., 1995, *A&A Rev.*, 6, 271
- Elbaz D., Cesarsky C. J., Chaniai P., Aussel H., Franceschini A., Fadda D., Chary R. R., 2002, *A&A*, 384, 848
- Elbaz D., Cesarsky C. J., Fadda D., Aussel H., Désert F. X., Franceschini A., Flores H., Harwit M. e. a., 1999, *A&A*, 351, L37
- Fioc M., Rocca-Volmerange B., 1997, *A&A*, 326, 950
- Fontana A., Salimbeni S., Grazian A., Giallongo E., Pentericci L., Nonino M., Fontanot F., Menci N., Monaco P., Cristiani S., Vanzella E., de Santis C., Gallozzi S., 2006, *A&A*, 459, 745
- Fontanot F., De Lucia G., Monaco P., Somerville R. S., Santini P., 2009, *MNRAS*, 397, 1776
- Fontanot F., Monaco P., Cristiani S., Tozzi P., 2006, *MNRAS*, 373, 1173
- Fontanot F., Monaco P., Silva L., Grazian A., 2007, *MNRAS*, 382, 903
- Fontanot F., Somerville R. S., Silva L., Monaco P., Skibba R., 2009, *MNRAS*, 392, 553
- Granato G. L., Lacey C. G., Silva L., Bressan A., Baugh C. M., Cole S., Frenk C. S., 2000, *ApJ*, 542, 710
- Gruppioni C., Lari C., Pozzi F., Zamorani G., Franceschini A., Oliver S., Rowan-Robinson M., Serjeant S., 2002, *MNRAS*, 335, 831
- Guiderdoni B., Rocca-Volmerange B., 1987, *A&A*, 186, 1
- Hauser M. G., Dwek E., 2001, *ARA&A*, 39, 249
- Kimm T., Somerville R. S., Yi S. K., van den Bosch F. C., Salim S., Fontanot F., Monaco P., Mo H., Pasquali A., Rich R. M., Yang X., 2009, *MNRAS*, 394, 1131
- Lagache G., Abergel A., Boulanger F., Désert F. X., Puget J.-L., 1999, *A&A*, 344, 322
- Lagache G., Dole H., Puget J.-L., 2003, *MNRAS*, 338, 555
- Lagache G., Dole H., Puget J.-L., Pérez-González P. G., Le Floc'h E., Rieke G. H., Papovich C., Egami E., Alonso-Herrero A., Engelbracht C. W., Gordon K. D., Misselt K. A., Morrison J. E., 2004, *ApJS*, 154, 112
- Le Floc'h E., Papovich C., Dole H., Bell E. F., Lagache G., Rieke G. H., Egami E., Pérez-González P. G. e. a., 2005, *ApJ*, 632, 169
- Leitherer C., Schaerer D., Goldader J. D., Delgado R. M. G., Robert C., Kune D. F., de Mello D. F., Devost D., Heckman T. M., 1999, *ApJS*, 123, 3
- Li A., Draine B. T., 2001, *ApJ*, 554, 778
- Lo Faro B., Monaco P., Vanzella E., Fontanot F., Silva L., Cristiani S., 2009, *MNRAS*, 399, 827
- Maiolino R., Schneider R., Oliva E., Bianchi S., Ferrara A., Mannucci F., Pedani M., Roca Sogorb M., 2004, *Nature*, 431, 533
- Mathis J. S., Mezger P. G., Panagia N., 1983, *A&A*, 128, 212
- Mo H. J., Mao S., White S. D. M., 1998, *MNRAS*, 295, 319
- Monaco P., 2004, *MNRAS*, 352, 181
- Monaco P., Fontanot F., Taffoni G., 2007, *MNRAS*, 375, 1189
- Monaco P., Murante G., Borgani S., Fontanot F., 2006, *ApJ*, 652, L89
- Panuzzo P., Bressan A., Granato G. L., Silva L., Danese L., 2003, *A&A*, 409, 99
- Panuzzo P., Granato G. L., Buat V., Inoue A. K., Silva L., Iglesias-Páramo J., Bressan A., 2007, *MNRAS*, 375, 640
- Popescu C. C., Misiriotis A., Kylafis N. D., Tuffs R. J., Fischera J., 2000, *A&A*, 362, 138
- Popescu C. C., Tuffs R. J., 2002, *MNRAS*, 335, L41
- Pozzetti L., Madau P., Zamorani G., Ferguson H. C., Bruzual A. G., 1998, *MNRAS*, 298, 1133
- Rieke G. H., Alonso-Herrero A., Weiner B. J., Pérez-González P. G., Blaylock M., Donley J. L., Marcillac D., 2009, *ApJ*, 692, 556
- Salpeter E. E., 1955, *ApJ*, 121, 161
- Sanders D. B., Mirabel I. F., 1996, *ARA&A*, 34, 749
- Schurer A., Calura F., Silva L., Pipino A., Granato G. L., Matteucci F., Maiolino R., 2009, *MNRAS*, 394, 2001
- Silva L., 1999, PhD thesis, AA(SISSA - Trieste (Italy))
- Silva L., Granato G. L., Bressan A., Danese L., 1998, *ApJ*, 509, 103
- Silva L., Schurer A., Granato G. L., Almeida C., Baugh C. M., Frenk C. S., Lacey C. G., Paoletti L., Petrella A., Selvestrel D., 2010, *ArXiv e-prints*
- Somerville R. S., Hopkins P. F., Cox T. J., Robertson B. E., Hernquist L., 2008, *MNRAS*, 391, 481
- Tuffs R. J., Popescu C. C., Völk H. J., Kylafis N. D., Dopita M. A., 2004, *A&A*, 419, 821
- Vega O., Silva L., Panuzzo P., Bressan A., Granato G. L., Chavez M., 2005, *MNRAS*, 364, 1286
- Viola M., Monaco P., Borgani S., Murante G., Tornatore L., 2008, *MNRAS*, 383, 777